Determination of the optimal forging conditions of a Cr-Mo-V high alloy steel through a microstructural, thermophysical and mechanical study

C. Bouffioux[1], M. Carton[2], J. Lecomte-Beckers[2], A-M. Habraken[1]

[1] *Department of Mechanics of Materials and Structures (M&S)*
University of Liège, 1, Chemin des Chevreuils, 4000 Liège, Belgium
URL: http://www.ulg.ac.be/matstruc/ e-mail:Chantal.Bouffioux@ulg.ac.be; Anne.Habraken@ulg.ac.be

[2] *Department of Aerospace, Mechanical and Materials Engineering Sciences (ASMA)*
University of Liège, 1, Chemin des Chevreuils, 4000 Liège, Belgium
URL:http://www.ulg.ac.be/metaux/ e-mail: Marc.Carton@ulg.ac.be; Jacqueline.Lecomte@ulg.ac.be

ABSTRACT: The forging process of cylinders requires the knowledge of material recrystallisation conditions to prevent crack appearance. Due to the continuous recrystallisation during forging, very large deformations can be applied as the generated dislocations do not yield to hardening but to recrystallisation phenomenon. This paper summarizes the data identification of a FEM recrystallisation model and defines the optimal forging process for one roll.

Key words: forging process, recrystallisation, thermophysical properties, mechanical tests, FEM simulation.

1 INTRODUCTION

To improve the fatigue properties and quality of rolls, new steel grades are developed. The studied Cr-Mo-V high alloy steel (semi HSS) is usually not used in forging process. It has been characterized in order to determine its ability to be forged and to determine the best range of temperature and strain rate to form rolls. This article describes the results of compression tests, metallographic analysis and measurements of thermophysical properties (conductivity, heat capacity, density). All these tests were required to identify the activation energy used in Zener-Hollomon parameter Z, the elasto visco plastic mechanical behavior law of Norton Hoff type and the thermal laws. They also allow to characterize the Recrystallisation phenomenon for this specific Cr-Mo-V high alloy steel. A recrystallisation model (1) is coupled with the thermo-mechanical model, it uses two curves defining the beginning and the end of the recrystallisation in the space "plastic strain-Ln Z".

2 COMPRESSION TESTS

In order to identify mechanical properties, to quantify the activation energy parameter and to study recrystallisation conditions, compression tests were performed at constant temperature T and at constant strain rate $\dot{\varepsilon}$ for different couple of values: T, $\dot{\varepsilon}$ and for different final strains. The stress strain curves show the influence of experimental conditions (figure 1).

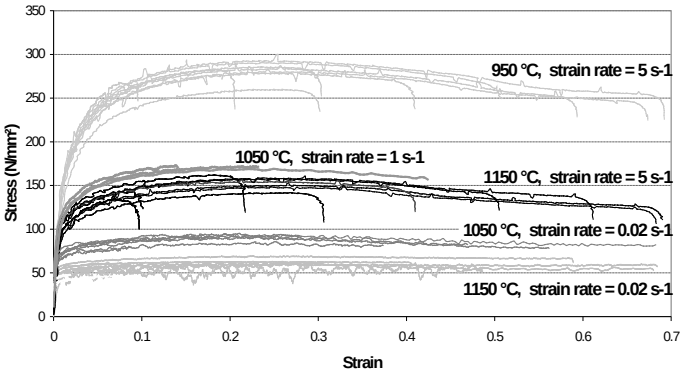

Fig. 1. stress-strain curves for different temperatures and strain rates

2.1 Mechanical law

The Norton Hoff law (equation 1) describes the material's behaviour with $\bar{\sigma}$, $\bar{\varepsilon}$ equivalent stress and strain, p_3, p_4, c_1, c_2, … c_6 material parameters:

$$\bar{\sigma} = K_0.\bar{\varepsilon}^{p_4}.\exp(-p_1.\bar{\varepsilon}).p_2.\sqrt{3}.(\sqrt{3}.\dot{\bar{\varepsilon}})^{p_3} \qquad (1)$$

$$p_1 = \left(\frac{T}{c_1}\right)^{c_2} + c_3 \qquad p_2 = \left(\frac{c_4}{T}\right)^2 - \frac{c_5}{T} + c_6$$

The law's parameters were optimised by Excel solver in order to obtain close agreement between Norton Hoff curves and compression tests results.

Table1. Optimised Norton Hoff law's parameters

K_0	C_1	C_2	C_3	C_4
150.0	1499.9	350.8	0.9100	4.215

C_5	C_6	P_3	P_4
-7036.3	-4.235	0.1107	0.216

The Zener-Hollomon parameter Z is defined by (equation 2). Its link with the maximum stress: σ_p (equation 3) allows to identify the activation energy parameter Q.

$$Z = \dot{\varepsilon}.\exp\frac{Q}{R.T} \qquad (2)$$

were R= gas constant (8.314 J/ mol.K),
T= temperature (K).

$$Z = A.(\sinh(\alpha.\sigma_p))^n \qquad (3)$$

were A, α and n = material data.

Q, A, α and n have been defined by Excel solver to fit all the experimental points: Q= 374 400 J/mol has been found.

3 METALLOGRAPHIC ANALYSIS

ε_C ε_s f (ln Z)

The compressed samples from section 2 were analysed in light microscopy. The HF etching was used to reveal the structure and especially grains of recrystallisation. An important quantity of large chromium carbides is present at grain boundaries. figure 2 shows that other smaller ones are observed in the matrix.

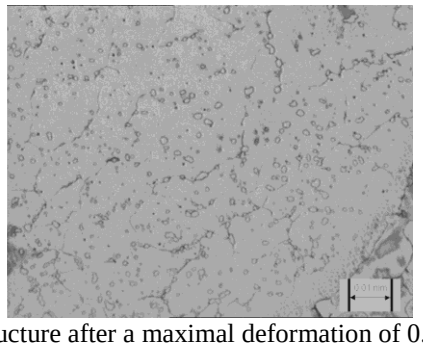

Fig. 2. Structure after a maximal deformation of 0.1, a strain rate of 0.02 s^{-1} and a temperature of 1050°C(X500)

The micrography clearly shows small precipitates and uniformly recrystallised grains distributed in the matrix. The same microstructural study was carried out for all compressed samples and the results are given in table 2, using the value of Q specified before.

Table2. Parameters of tests and recrystallisation state

Strain Rate (s^{-1})	ε	T°(°C)	Recrystallisation state	Ln Z
0.02	0.5	849	No	36.24
0.02	0.7	849	No	36.24
0.02	0.55	914	Little	34.04
0.02	0.1	992	No	31.7
0.02	0.1	1050	Yes	30.14
1	0.15	1050	No	34.05
1	0.45	1050	Average	34.05
0.02	0.5	1050	Yes	30.14
0.02	0.7	1050	Yes	30.14
0.02	0.1	1098	Yes	28.95
0.02	0.02	1150	Little	27.25
0.02	0.05	1150	Little	27.25
0.02	0.08	1150	Little	27.25
0.02	0.55	1150	Yes	27.75

The table 2. shows that the higher temperature, the larger the recrystallisation. On the other hand, the higher strain rate, the smaller the recrystallisation.
Figure 3 proposes a representation of the different areas corresponding to different states of recrystallisation.
Critical curves show the limit conditions generating a total or a non-recrystallisation. The results of all tests are shown in figure 3.

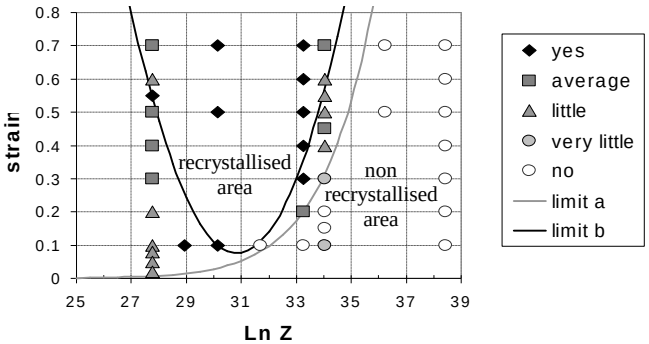

Fig. 3. Different recrystallisation area in terms of compression tests conditions.

Limit a curve defines the recrystallisation beginning and limit b its end. The recrystallised fraction X is classically calculated by Avrami law (equation 4).

$$X = 1 - \exp[-3.(\frac{\varepsilon - \varepsilon_c}{\varepsilon_s - \varepsilon_c})^n] \qquad (4)$$

were n = 5.284.

4 THERMOPHYSICAL PROPERTIES

Thermal parameters must be known for numerical simulations of the material during processing. Hence dilatation, specific heat, thermal diffusivity and thermal conductivity were determined.

4.1 Dilatation $\Delta L/L_0$

Two samples corresponding to the radial and axial direction of the investigated roll were heated and cooled down with a rate of ten degrees per minute, with a maximum temperature value of 1200°C (see figure 4).

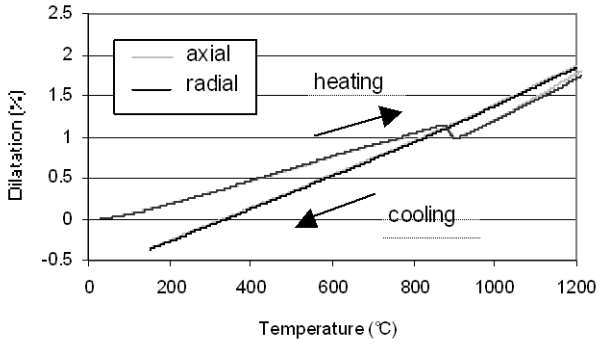

Fig. 4. Dilatation and contraction in terms of temperature during heating and cooling.

The values given here represent the relative dilatation $\Delta L/L_0$. During heating, a peak is obtained at 875°C corresponding to the austenitic transformation. A slight difference is observed between the axial and radial directions at 1200°C, whereas the signal during cooling is linear.

4.2 Density $\rho(T)$

The density evolution in terms of temperature is shown in figure 5.

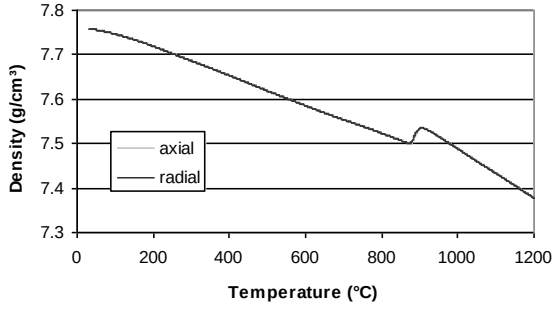

Fig. 5. Density in terms of temperature.

The density ρ decreases from 7.75 g/cm³ (at room temperature) to 7.38 g/cm³ (at 1200°C). As the density is directly calculated from dilatation values, the peak at 875°C is also observed here.

4.3 Specific heat C_p

The analysed sample was heated and cooled down with a rate of 10 degrees per minute between room temperature and 1200°C.

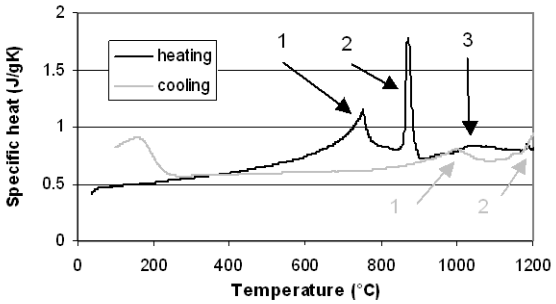

Fig. 6. Specific heat during heating and cooling in terms of temperature.

During heating, three peaks were obtained, respectively at 752°C, 872°C (corresponding to the austenitic transformation) and 1180°C (carbides dissolution). After heating, the sample was immediately cooled down.

During cooling, two peaks at 1150°C and 1000°C were obtained, corresponding to carbides precipitations.

4.4 Thermal conductivity $\chi(T)$

The thermal diffusivity was measured during heating. Knowledge of thermal diffusivity, density and specific heat allows the determination of thermal conductivity shown in figure 7.

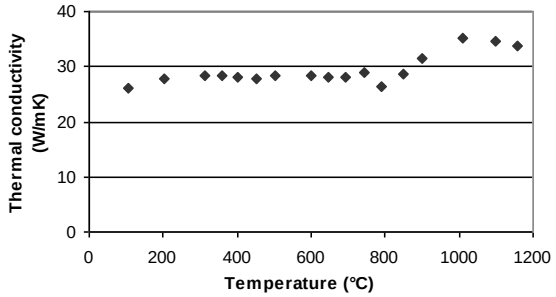

Fig.7. Thermal conductivity in terms of temperature

The thermal conductivity increases from 26.1 W/mK to 33.7 W/mK, with a peak at about 750°C (austenitic transformation).
It is important to note that specific heat and therefore thermal conductivity values are given taking into account the quantity of heat released during the solid phase transformations.

5 OPTIMAL FORGING CONDITIONS

The recrystallised areas in figure 3 are examined for low strains, according to results of some forging simulations. As we can see in figure 8, Ln Z is the determinant factor to determine weather or not recrystallisation occurs.

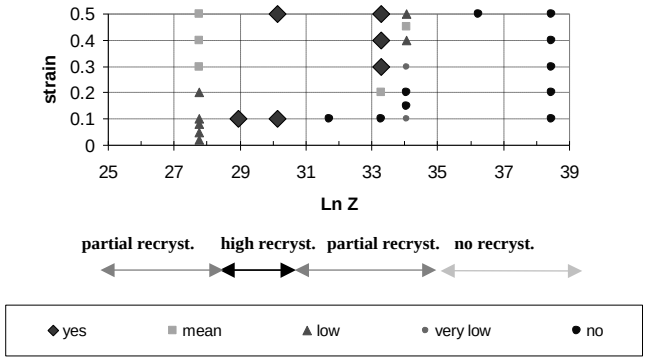

Fig.8. Recrystallisation state

This graphic identifies the optimum Zener parameter to yield to recrystallisation in a test where Ln Z is a constant. It helps to define the best range of temperature and strain rate to forge rolls. However, as the material is far from a loading at constant value of Ln Z, simulations under different assumptions are required to identify actual optimal conditions.

6 PROCESS SIMULATION

A simulation allows to verify the state of recrystallisation once the initial temperature and punch velocity are choosen. The validity of 3D simulation was already investigated in previous study [2]. We've considered an initial temperature field variable with the radius [1134 at the surface layer, 1425 in the center] K. This field was computed under the assumption of an initial air cooling.

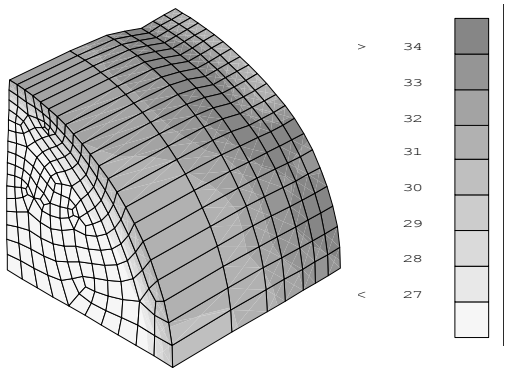

Fig.9. Values of Ln Z at the end of forging

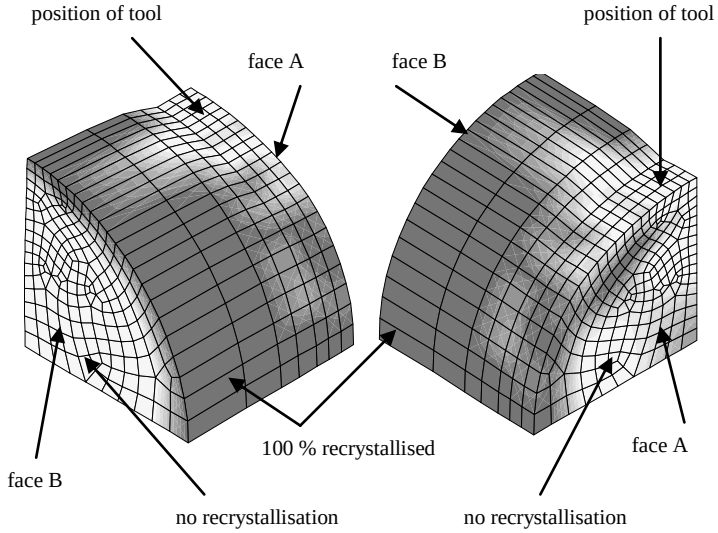

Fig.10. Results: recrystallisation state.

Due to symmetry, only a eighth of roll is considered. Face A is fixed while face B is free (figure 10). The tool reduces the diameter from 1385 mm to 1235 mm and the forging time is 3.75 s.
The recrystallised area is situated near the surface except beside the tool, where $29 \leq \text{Ln } Z \leq 33$.

7 CONCLUSIONS

The data obtained in this study allow to define the best range of temperature and strain rate to forge rolls. The first simulation with current industrial forging conditions verifies the state of recrystallisation. Other simulations will compare different forging conditions and will help to choose the optimal initial temperature and tool speed.

ACKNOWLEDGEMENTS

AM Habraken is a Senior Research Associate of National Fund for Scientific Research (Belgium), and thanks this research fund (FNRS) for support.
The Région Wallonne provides financial support (project RW 981/3793) and Åkers actively collaborates in the research. The authors thank both of them

REFERENCES

1. A.M. Habraken, J.F. Charles, J. Wegria, S. Cescotto, Dynamic Recrystallisation during Zinc Rolling, *Int. J. of Forming Processes*, 1, 1998 (20 pages).
2. J.F. Charles, S. Castagne, L. Zhang, A.M. Habraken, S. Cescotto, Numerical modeling of the forging process of rolls for rolling mills, 8th int. Conf on Metal Forming, 3-7 September 2000 *Metal Forming 2000* M. Pietrzyk, J Kusiak, J Majta, P Hartley I Pillinger Editors, BALKEMA, 625-631.